# Microstructural Evolution and Physico-Mechanical Response of Cement-Bonded Fiberboards: A Comparative Study on Cement Type and Fiber Ratio

Emrecan Arpaci , Sebnem S. Arpaci * , Ergun Guntekin

Posted Date: 28 January 2026

doi: 10.20944/preprints202601.2020.v1

Keywords: wood-cement composites; physico-mechanical properties; microstructural characterization; fiber-matrix interface; thermal conductivity

 doi:10.20944/preprints202601.2020.v1



*Article*

# Microstructural Evolution and Physico-Mechanical Response of Cement-Bonded Fiberboards: A Comparative Study on Cement Type and Fiber Ratio

**Emrecan Arpaci, Sebnem S. Arpaci * and Ergun Guntekin**

Department of Forest Industry Engineering, Bursa Technical University, Bursa 16310, Turkey

* Correspondence: sebnem.arpaci@btu.edu.tr

**Abstract**

This study investigates the critical interplay between cement grade (32.5, 42.5, 52.5) and fiber/cement ratio (1/2 to 1/5) in determining the performance of cement-bonded fiberboards. Experimental results highlighted a fundamental trade-off: while reducing the fiber content significantly enhanced mechanical strength and moisture resistance, it naturally diminished thermal insulation capabilities. The analysis identified the 42.5 cement at a 1/4 ratio as the optimal formulation, offering the most effective balance between structural integrity and physical stability. To understand the mechanism behind this performance, the study employed multi-scale characterization using FTIR, XRD, and SEM. These analyses revealed that the superior properties of the optimal formulation stem from a denser hydration product network and improved fiber encapsulation. Specifically, the 42.5 cement facilitated a more robust Calcium-Silicate-Hydrate (C-S-H) gel formation compared to the 32.5 types, creating a stronger fiber-matrix interface. These findings provide a scientific basis for tailoring fiberboard production, demonstrating that material properties can be precisely engineered for either load-bearing or insulating applications.

**Keywords:** wood-cement composites; physico-mechanical properties; microstructural characterization; fiber-matrix interface; thermal conductivity

## 1. Introduction

Wood-based composite materials offer excellent potential for construction applications due to their advantages, including being lightweight yet strong, design flexibility, energy efficiency, and environmental friendliness. Consequently, natural fiber-based composites have become a popular alternative to traditional materials, marking an important step towards a more sustainable construction sector. Cement-bonded wood composites, utilizing materials like wood wool, fiber, and chips, have been used in the building industry for over a century.

Amid increasing environmental concerns, there has been a growing interest in renewable raw materials, leading to the development of cementitious boards reinforced with natural fibers [1]. Fiber-reinforced cement boards are known for their durability and versatility, commonly used in roofing and exterior siding. They offer a practical building solution that integrates strength, longevity, weather resistance, and ease of handling. Research indicates that adding fibers, typically around 10% by weight, enhances the mechanical properties of these boards, including flexural strength, toughness, and impact resistance [2,3]. Additionally, these boards can reduce thermal conductivity (0.217-0.430 W/mK) [4] and improve sound absorption [5].

Portland cement (PC), the primary binder, is categorized by its minimum 28-day compressive strength: 32.5, 42.5, and 52.5 MPa [6–8]. Class 32.5 cements are suitable for applications where high early strength is not required. Class 42.5 is widely used for concrete requiring compressive strength over 30 N/mm², while Class 52.5 is used for applications demanding even faster setting and higher initial strength, such as in precast elements.

 doi:10.20944/preprints202601.2020.v1



Class 32.5 cements are recommended for applications where high early-age strength is not a necessity, in average ambient temperatures (10°-15°C) and for structures with common thicknesses (< 50 cm). Cements belonging to the 42.5 strength class are widely employed in cases where the required 28-day concrete compressive strength must exceed 30 N/mm² (higher than class C25/30 as per NBN B 15-001). These cements are also suitable for use in lower temperature environments. Class 52.5 cements are utilized for applications demanding an even greater initial strength than that of Class 42.5 cements. For instance, they may be used for the rapid de-moulding of precast elements. 52.5 is a fast-setting cement with high strength characteristics, but the most used cement type today is 42.5.

While extensive research has focused on optimizing CFBs through alternative fibers, chemical accelerators, or manufacturing parameters [9,10], the cement binder itself is often treated as a constant, typically a standard CEM I or CEM II 42.5 R cement [11]. This has created a critical knowledge gap, as there is a lack of systematic research comparing different Portland cement strength classes within a unified wood-fiber composite framework. The specific interactions of these cements with lignocellulosic inhibitors and their influence on the fiber-matrix interfacial transition zone (ITZ) remain poorly understood.

Consequently, a critical knowledge gap persists: there is a notable lack of systematic research comparing the performance of different standard Portland cement strength classes (e.g., 32.5, 42.5, and 52.5) within a unified wood-fiber composite framework. While the properties of these cements in conventional concrete are well-documented [6–8], their specific interactions with lignocellulosic inhibitors and their influence on the complex fiber-matrix interfacial transition zone (ITZ) remain poorly understood. This oversight limits the potential for true performance optimization, as the industry continues to rely on convention rather than comparative data for binder selection.

This research directly addresses this gap by systematically analyzing how varying both the Portland cement strength class and the fiber/cement ratio impacts the critical properties of CFBs. By integrating a comprehensive suite of characterization methods—from macroscopic mechanical, physical, and thermal testing to microscopic (SEM) and chemical (FTIR, XRD) analyses this study aims to decouple the effects of cement type and fiber ratio. The findings will provide a foundational dataset and a practical roadmap for the targeted design of more durable and high performance CFB.

## 2. Materials and Methods

### *2.1. Materials*

In this study, carefully selected materials were used for the production of experimental CFB. Three different types of Portland Cement (PC) (CEM II 32.5 R, CEM II 42.5 R, and CEM II 52.5 R) were sourced from a commercial supplier. These cement types were selected to comprehensively evaluate the effect of cement grade on CFB properties by offering different early and final strength developments.

As a reinforcement element, pine (*Pinus* spp.) wood fibers obtained from a commercial MDF (Medium Density Fiberboard) manufacturer were used. The main fibers forming the basis of the boards were obtained from softwood-based MDF production waste and had an average length of 758 µm and a diameter of 28 µm. The chemical composition of the pine fibers is presented in Table 1.

**Table 1.** Chemical composition of the pine fibers.

| Fiber Type | Cellulose (%) | Hemicellulose (%) | Lignin (%) | Ash/Extractives (%) |
|---|---|---|---|---|
| Pine | 45.2 | 25.4 | 27.9 | 1.5 |

The fibers were conditioned to an appropriate moisture content before production to ensure homogeneous distribution. It is well-established that wood extractives, such as hemicelluloses and sugars, significantly inhibit the hydration of Portland cement, leading to prolonged setting times and

 doi:10.20944/preprints202601.2020.v1



reduced final strength [10,12]. To counteract this inhibitory effect, Calcium Chloride ($CaCl_2$) was used as a setting accelerator. $CaCl_2$ is widely preferred in wood-cement composites for its ability to promote hydration and overcome the retarding effects of wood extractives [10]. Analytically pure $CaCl_2$ (Merck Co, Germany) was used at a dosage of 5% by weight of cement. This dosage was chosen to ensure a rapid setting process, critical for achieving a strong fiber-matrix bond and high early strength [12]. Distilled water was used in all mixtures.

### *2.2. Determination of Cement Fineness (Blaine Test)*

he specific surface area (fineness) of the cements was determined using a Blaine air permeability apparatus in accordance with the EN 196-6 standard. The test is based on the air permeability principle derived from the Kozeny-Carman equation. A specific mass of the cement sample was placed into a standard cell and compressed to form a bed with a known porosity (ε=0.500). The time (*t*, in seconds) required for a fixed volume of air to pass through this cement bed was measured. The specific surface area (*S*) was calculated using the formula: $S = (K * \sqrt{t}) / p$. All measurements were repeated three times, and the average values were recorded in $cm^2/g$.

*Where P: Represent the density of the tested cement in $g/cm^3$, K: Represents the apparatus constant, previously determined using a standard reference cement with a known surface area*

### *2.3. Cement Particle Size Distribution (PSD) Analysis*

The PSD of cement samples was determined using a laser diffraction particle size analyzer (Malvern Mastersizer 3000) following ISO 13320. Samples were dispersed in ethanol to prevent agglomeration. The analysis reported key parameters including D10, D50, D90, and Span (*[D90-D10]/D50*)).

### *2.4. Board Manufacturing*

A total of 12 different board formulations were produced using three cement types and four fiber/cement ratios (1:2, 1:3, 1:4, and 1:5 by weight). The amount of distilled water was calculated using the formula proposed by Fuwape [13] to achieve optimal workability and density: *Water (L) = 0.35 C + (0.30 – MC) W.*

*Where C = cement weight (kg) , MC (%) = wood fibers moisture content (oven-dry basis), W = oven-dry wood fiber weight (kg).*

The wood fibers, cement, and $CaCl_2$ were mixed dry in a mechanical mixer until homogeneous. Subsequently, the calculated amount of water was slowly added to form a homogeneous paste. The mixture was evenly distributed into a metal frame (35 x 30 x 1.2 cm) and compressed under a hydraulic press at 40 bar for 24 hours. The demolded wet boards were cured under standard laboratory conditions (23 ± 2 °C and 65 ± 5% relative humidity) for 28 days.

### *2.5. Determination of Density*

The density of the cement-bonded fiberboards was determined in accordance with the TS EN 323 standard. The dimensions (length, width, thickness) of each sample were measured using a digital caliper with a precision of ±0.01 mm to calculate the volume. Density values were obtained by dividing the mass by the volume. The reported density for each formulation represents the average of three replicates.

### *2.6. Modulus of Rupture and Modulus of Elasticity*

MOR and MOE were determined via a three-point bending test according to TS EN 310. Samples were conditioned at 23 ± 2°C and 50 ± 5% relative humidity for 72 hours prior to testing. Tests were performed on a universal testing machine with 8 replicates per group.

### *2.7. Determination of Water Absorption and Thickness Swelling Values*

 doi:10.20944/preprints202601.2020.v1



WA and TS were determined according to TS EN 317. Eight replicate samples per group were conditioned and immersed in water for 24 hours. Initial and final mass and thickness measurements were recorded to calculate the percentage changes.

### *2.8. Thermal Conductivity*

TC ($\lambda$) was measured using a LASER COMP. - FOX 314-95ET device according to ASTM C1113-99:2004. Measurements were conducted on 10x10 cm samples to evaluate thermal insulation performance.

### *2.9. Fourier Transform Infrared Spectroscopy*

Functional group analysis was performed using a Bruker Tensor 37 spectrometer equipped with an ATR (Attenuated Total Reflectance) module. Spectra were recorded in the range of 4000-400 $cm^{-1}$ with a resolution of 4 $cm^{-1}$ and 32 scans. Data were analyzed using Bruker OPUS software. Six measurements were taken per sample to ensure reliability.

### *2.10. X-Ray Diffraction*

XRD analysis was performed on powdered samples taken from the fracture zones after bending tests. Samples were vacuum-dried at 80 °C for 24 hours. The analysis was conducted using a Bruker D8 Advance diffractometer (Cu-K$\alpha$ radiation, Ni filter) with a scanning speed of 0.5°/min, a range of 10°-100° (2$\theta$), and a step size of 0.02°.

### *2.11. Scanning Electron Microscope*

Microstructure and fiber-matrix interfaces were examined using SEM on 1 $mm^3$ samples taken from fracture surfaces. Specimens were gold-palladium (Au/Pd) coated prior to imaging to prevent charging.

### *2.12. Data Analysis*

Statistical analysis was conducted using IBM SPSS Statistics 22. One-Way Analysis of Variance (ANOVA) was applied to determine the effects of variables on board properties, with a significance level set at $\alpha$=0.05.

## 3. Results

The properties of the cement used in this study are presented in detail in Table 2. The chemical composition of the raw materials was accurately determined using X-ray fluorescence (XRF) analysis. XRF analysis is a widely used and reliable method for determining the major and trace element compositions of cement and other inorganic binders [14,15]. As a result of this analysis, the main chemical compounds found in the cement content include silica ($SiO_2$), alumina ($Al_2O_3$), iron (III) oxide ($Fe_2O_3$), and calcium oxide (CaO).

**Table 2.** Chemical and physical characteristics of Portland cement.

| Cement type | Chemical composition (%) | | | | | | |
|---|---|---|---|---|---|---|---|
| CEMII | $SiO_2$ | $Al_2O_3$ | $Fe_2O_3$ | CaO | MgO | $SO_3$ | other |
| 52.5 | 18.4 | 4.14 | 0.360 | 71.0 | 1.13 | 4.42 | 0.55 |
| 42.5 | 24.6 | 6.74 | 4.15 | 57.5 | 0.774 | 4.29 | 1.946 |
| 32.5 | 18.5 | 3.0 | 2.2 | 60.5 | 0.9 | 2.9 | 2.1 |

The ratios of these oxides directly affect the hydration reactions, setting time, and final mechanical properties of the cement. For example, CaO is the main component of Portland cement and plays a crucial role in the formation of strength-giving products such as calcium silicate hydrate

 doi:10.20944/preprints202601.2020.v1



(C-S-H) gel. $SiO_2$ is critical for the formation of calcium silicate phases ($C_3S$ and $C_2S$), which provide the hydraulic properties and strength development of the cement. $Al_2O_3$ and $Fe_2O_3$ contribute to the early strength and setting properties of the cement by forming tricalcium aluminate ($C_3A$) and tetracalcium aluminoferrite ($C_4AF$) phases, respectively [16]. This raw material characterization has provided essential data to relate the variations in the performance of the produced cement-based fiberboards to the chemical composition of the cement. Similarly, many studies on fiber-reinforced cement composites have thoroughly examined the chemical composition of the binders [17,18]. This approach supports the methodological rigor of our study and the reliability of the results obtained. Some physical properties of the experimentally manufactured CFB are presented in Table 3.

**Table 3.** Some physical properties of CFB panels.

| | Cement type | 1/2 | 1/3 | 1/4 | 1/5 |
|---|---|---|---|---|---|
| d (g/cm³) | 32.5 | 1.28 ± 0.08 | 1.23 ± 0.05 | 1.56 ± 0.08 | 1.49 ± 0.06 |
| | 42.5 | 1.06 ± 0.04 | 1.39 ± 0.07 | 1.57 ± 0.05 | 1.68 ± 0.09 |
| | 52.5 | 1.10 ± 0.09 | 1.40 ± 0.07 | 1.56 ± 0.08 | 1.67 ± 0.05 |
| WA (%) | 32.5 | 35.1 ± 2.5 | 30.5 ± 2.1 | 25.8 ± 1.8 | 22.4 ± 1.6 |
| | 42.5 | 32.5 ± 2.2 | 28.1 ± 1.9 | 23.2 ± 1.6 | 20.1 ± 1.4 |
| | 52.5 | 30.8 ± 2.1 | 26.5 ± 1.8 | 22.1 ± 1.5 | 18.9 ± 1.3 |
| TS (%) | 32.5 | 2.8 ± 0.2 | 2.4 ± 0.2 | 2.0 ± 0.1 | 1.8 ± 0.1 |
| | 42.5 | 2.5 ± 0.2 | 2.1 ± 0.1 | 1.7 ± 0.1 | 1.5 ± 0.1 |
| | 52.5 | 2.3 ± 0.1 | 1.9 ± 0.1 | 1.6 ± 0.1 | 1.3 ± 0.1 |

### *3.1. Density*

As observed in Table 3, the density of the boards generally increased with an increase in cement content relative to the fibers. This is attributed to the higher specific gravity of the cement matrix compared to wood fibers. For the 42.5 cement type, density values rose from 1.06 g/cm³ to 1.68 g/cm³ as the fiber/cement ratio decreased from 1/2 to 1/5. This finding is consistent with previous studies indicating that increasing the binder content directly enhances composite density [19].

Notably, the 42.5 cement exhibited higher density values compared to other types, particularly at lower fiber/cement ratios. Statistical analysis (ANOVA) confirmed that both cement type and fiber/cement ratio had a significant effect on density ($p<0.05$). The Duncan multiple comparison test revealed specific differences between groups: the boards produced with 42.5 and 52.5 cements at a 1/5 ratio (1.68 and 1.67 g/cm³, respectively) formed a statistically homogeneous group, whereas the density of the boards produced with 32.5 cement (1.49 g/cm³) was significantly lower.

### *3.2. Hygroscopic Properties*

TS and WA values are critical for the dimensional stability of cement-bonded fiberboards. As shown in Table 3 and Figure 1, a significant decrease in both TS and WA values was observed with the reduction of the fiber/cement ratio. This improvement is due to the hydrophobic nature of the cement matrix, which encapsulates the fibers and limits the water uptake of hydrophilic hydroxyl groups. These results align with findings in the literature [20–22].

Higher strength class cements (42.5 and 52.5) demonstrated superior hygroscopic performance due to the formation of a denser and less porous matrix. ANOVA results confirmed that both cement type and fiber ratio significantly affected water absorption ($p<0.05$). The Duncan test revealed

 doi:10.20944/preprints202601.2020.v1



significant differences among cement grades at a fixed fiber ratio; for instance, at a 1/3 ratio, the WA values for 32.5, 42.5, and 52.5 cements were 30.2%, 27.5%, and 24.1%, respectively, indicating that they belong to statistically distinct groups.

A similar trend was observed for TS values. The group with the best performance (52.5 cement at 1/5 ratio) exhibited a swelling value of 1.3%, which was statistically distinct from the highest swelling group (32.5 cement at 1/2 ratio, 2.8%). This demonstrates a strong correlation between the water absorption capacity and the dimensional stability of the boards.

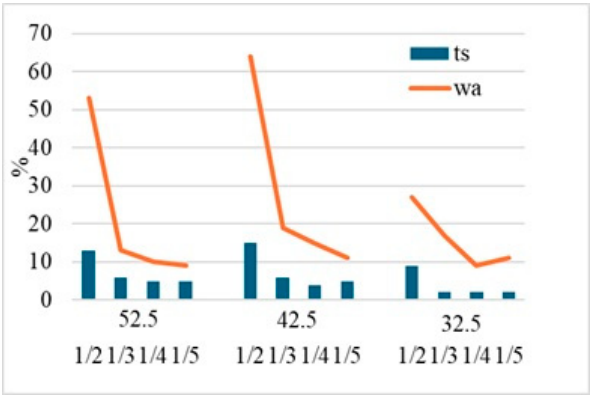


**Figure 1.** Effects of fiber / cement ratio and cement type on TS and WA of the boards.

*3.3. Flexural Properties*

The MOR and MOE values clearly demonstrate the critical impact of the fiber/cement ratio and cement type on mechanical performance (Table 4 and Figures 2 and 3). As a general trend, a decrease in the fiber/cement ratio (increasing cement content) is associated with a significant increase in both MOR and MOE values. This indicates the vital contribution of the cement matrix to the load-bearing capacity and rigidity of the board. Enough cement better encapsulates the fibers, creating a homogeneous matrix and strengthening the bond at the fiber-matrix interface [1].

**Table 4.** Some mechanical properties of CFB panels.

| | Cement type | 1/2 | 1/3 | 1/4 | 1/5 |
|---|---|---|---|---|---|
| MOR (N/mm²) | 32.5 | 1.69 ± 0.37 | 4.35 ± 0.85 | 10.71 ± 0.81 | 9.86 ± 0.44 |
| | 42.5 | 2.69 ± 0.21 | 6.93 ± 1.43 | 12.77 ± 0.78 | 12.49 ± 0.58 |
| | 52.5 | 2.09 ± 0.22 | 11.25 ± 2.19 | 12.02 ± 0.89 | 11.5 ± 1.0 |
| (MOE) (N/mm²) | 32.5 | 953 ± 412 | 1428 ± 229 | 4578 ± 547 | 4939 ± 548 |
| | 42.5 | 313 ± 104 | 2628 ± 587 | 5561 ± 657 | 6388 ± 749 |
| | 52.5 | 482 ± 229 | 3919 ± 518 | 5247 ± 592 | 6199 ± 650 |

The highest MOR and MOE values were generally obtained in boards with fiber/cement ratios of 1/4 and 1/5. For the 42.5 cement type, the MOR peaked at 12.77 N/mm² with a 1/4 ratio, while the MOE reached 5561 N/mm². With the same cement at a 1/5 ratio, the highest MOE value of 6388 N/mm² was recorded. These findings align with literature emphasizing that optimal fiber content is critical for maximum strength; excessive fiber content prevents adequate encapsulation by the matrix, resulting in weak interfaces [23].

 doi:10.20944/preprints202601.2020.v1



Among the cement types, 42.5 and 52.5 generally provided higher mechanical values compared to 32.5. This is explained by the ability of higher strength class cements to form a denser and more robust matrix [24]. Specifically, the expansion in wood volume relative to the cement matrix at high fiber ratios reduces bond strength.

Statistical analysis (ANOVA) confirmed that both cement type and fiber/cement ratio had a significant effect on the mechanical properties ($p<0.05$). To illustrate the magnitude of this effect, the extreme examples are telling: The group using 42.5 cement with a 1/4 ratio yielded the highest MOR (12.77 N/mm²), whereas the group using 32.5 cement with a 1/2 ratio yielded the lowest (1.69 N/mm²), placing them in statistically distinct classes. A similar trend was observed for MOE; particularly at the 1/5 ratio where rigidity is maximized, the value obtained with 42.5 cement (6388 N/mm²) was significantly higher than that of 32.5 (4939 N/mm²).

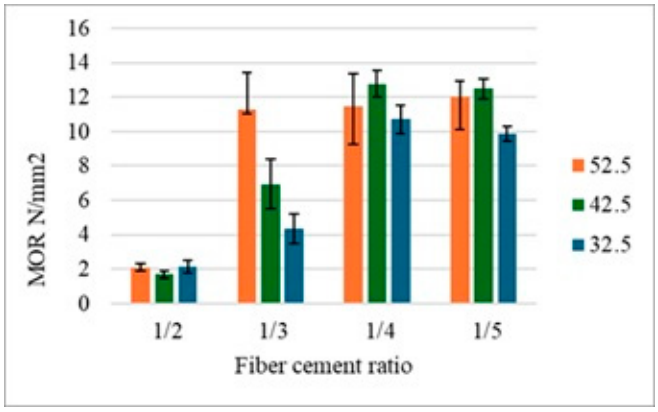


**Figure 2.** Effects of fiber / cement ratio and cement type on MOR of the boards.

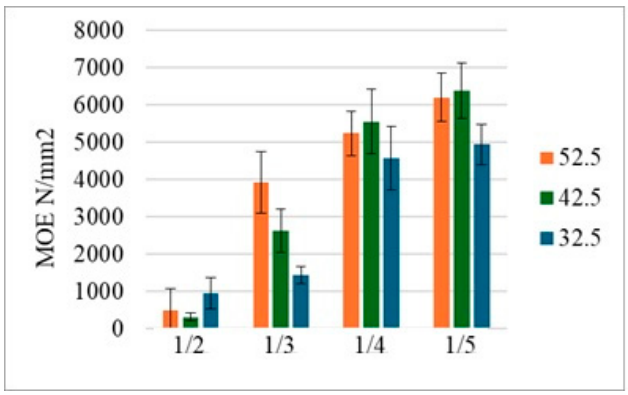


**Figure 3.** Effects of fiber / cement ratio and cement type on MOE of the boards.

### *3.4. Thermal Conductivity*

The Thermal Conductivity (TC, $\lambda$) values are critical for evaluating the insulation performance of CFB. Figure 4 presents the TC values obtained for different cement types and fiber/cement ratios.

Generally, an increasing trend in thermal conductivity is observed as the fiber/cement ratio decreases (cement content increases). This is an expected outcome, as the cement matrix has significantly higher thermal conductivity compared to wood fibers, which act as natural insulators due to their porous structure [25]. The TC values in this study ranged from approximately 0.22 W/mK for high-fiber boards (1/2 ratio) to 0.50 W/mK for low-fiber boards (1/5 ratio).

To assess the practical significance of these results, it is crucial to compare them with common building materials. Traditional clay brick typically has a thermal conductivity of 0.6–1.0 W/mK, and standard concrete is usually above 1.5 W/mK. In this context, all fiberboards produced in this study offer considerably better thermal insulation. More importantly, the lowest TC values achieved (≈0.22

 doi:10.20944/preprints202601.2020.v1



W/mK) are highly competitive, approaching those of lightweight insulation materials like aerated autoclaved concrete (AAC), which typically ranges from 0.1–0.2 W/mK.

Furthermore, the CFBs manufactured in this study exhibited a lower thermal conductivity coefficient than that reported for other cement-bonded particleboards (0.26 W/mK) [26], indicating superior insulation capability. This positive effect of fiber content on thermal insulation is consistent with findings in the literature [27,28]. These results underscore the importance of optimizing the fiber/cement ratio not only for mechanical properties but also for creating energy-efficient building materials.

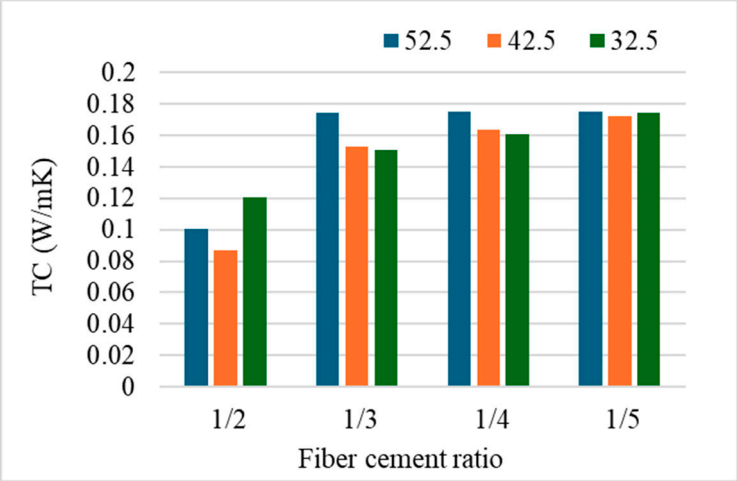


**Figure 4.** Effects of fiber / cement ratio and cement type on thermal conductivity of the boards.

*3.5. A Deeper Analysis of Interfacial Performance and the Superiority of 42.5*

While the general trends observed in this study—such as increased mechanical performance with higher cement content—are consistent with the literature [19,20], a simple recitation of these results is insufficient. A deeper discussion is required, particularly concerning the counter-intuitive finding where 42.5 cement, in certain formulations (notably the 1/4 fiber/cement ratio), demonstrated mechanical properties superior to those of the higher-strength grade 52.5. This observation challenges the simplistic assumption that a higher cement strength class automatically translates to a better composite. The explanation likely lies in a complex interplay of hydration kinetics, particle characteristics, and the resulting C-S-H morphology at the fiber-matrix interface.

The assertion that 42.5 and 52.5 cements form a "denser and more robust matrix" [24] is correct, but it does not fully explain the nuanced differences between them. The superiority of 42.5 cannot be attributed solely to the quantity of C-S-H gel, but rather to its quality and morphology at the crucial interface with the wood fibers. We propose three interconnected mechanisms to explain this phenomenon:

***Optimal hydration kinetics and interfacial zone development:*** CEM II 52.5 cements are characterized by higher fineness (Blaine) and a greater proportion of tricalcium silicate ($C_3S$), leading to very rapid hydration and early strength gain [14,16]. While beneficial in conventional concrete, this rapid reaction can be detrimental in a wood-cement composite. A very fast hydration process might create a dense, but brittle and poorly adhered, shell of C-S-H around the wood fibers. This rapid "encasement" may prevent a deeper, more gradual penetration of hydration products into the porous, cellular structure of the wood fiber surface, resulting in a weaker mechanical interlock. In contrast, the more moderate hydration rate of 42.5 likely allows for a more controlled development of the interfacial transition zone (ITZ). This enables hydration products to form not just on the fiber surface, but partially within its voids, creating a more integrated and tougher bond that is better at transferring stress from the matrix to the fibers [29].

 doi:10.20944/preprints202601.2020.v1



***The influence of chemical composition on C-S-H morphology:*** As highlighted by Scrivener et al. (2019) [16], the microstructure of cement paste is significantly influenced by its minor components, particularly alumina. Portland cements are not pure $C_3S$; their aluminate and ferrite phases ($C_3A$ and $C_4AF$) alter the growth and distribution of the C-S-H gel. It is plausible that the specific chemical composition of the 42.5 used in this study resulted in a C-S-H morphology that is more advantageous for bonding with organic fibers. For instance, a less "foil-like" and more "spiky" or fibrillar C-S-H nanostructure could provide superior mechanical anchoring to the cellulose fibers [27]. The high Si-O and Al-O intensity ratios observed in our FTIR analysis for the 42.5 sample (1/4 ratio) strongly support this hypothesis, indicating the formation of a chemically distinct and potentially more effective C-S-H and C-A-S-H network.

***The role of particle size distribution and matrix homogeneity:*** Beyond chemical composition, the physical properties of cement play a critical role [30]. As outlined in Table 5, optimal composite performance is often achieved not with the finest powder, but with a well-graded particle size distribution (PSD) that ensures efficient particle packing [24,31]. The superiority of the 42.5 cement in our study strongly supports this principle.

This difference in distribution is not merely qualitative; it is quantitatively visualized in the PSD curves presented in Figure 5. Analysis of these curves provides clear, numerical evidence for the descriptions in Table 5. Specifically, the graph reveals that:

- 52.5 cement has approximately 70% of its particle volume under 10 μm, confirming its "fine and narrow" character.
- 42.5 cement demonstrates a true "well-graded" structure, with significant particle volumes distributed across the entire spectrum: from fine (≈20% < 5 μm) to medium (≈45% between 5-20 μm) and coarse (≈35% > 20 μm).
- 32.5 cement is confirmed as "coarser," with over 60% of its volume residing in particles larger than 20 μm.

**Table 5.** Fineness and particle size distribution parameters of cement samples.

| Cement Type | Blaine Fineness ($cm^2/g$) | PSD | Discussion |
|---|---|---|---|
| 32.5 | 3600-3800 | Coarser and wider distribution. | Lower fineness leads to a slower hydration reaction and consequently lower early-age strength [30]. |
| 42.5 | 3900-4200 | Well graded (wide distribution). Contains a balanced mix of both fine and medium-sized particles. | The well-graded structure allows for the most efficient packing of particles, creating a less porous (low porosity) and homogeneous matrix [31,32]. |
| 52.5 | 4300-4800 | Very fine and narrow distribution. Most particles are of a similar and very small size. | The highest fineness results in very rapid hydration and high early strength. However, this can lead to a brittle interface with thermal stresses and micro-cracks around the wood fiber due to rapid heat release [33]. |

A second critical advantage of a well-graded PSD is the management of hydration heat. Cements with higher strength classes, typically featuring finer grinding—a characteristic now quantitatively confirmed for 52.5 by Figure 5—tend to release hydration heat more rapidly and at higher levels [34]. This rapid heat increase can cause thermal stresses, especially between the inner and outer parts of the composite, leading to micro-cracks in the interfacial transition zone (ITZ) [33]. These micro-cracks create weak points that prevent the material from reaching its potential strength.

 doi:10.20944/preprints202601.2020.v1



In contrast, the more controlled and slower heat release of 42.5 reduces this thermal shock effect and allows for the formation of a more robust, damage-free interface. This directly contributes to the material's ultimate mechanical strength and durability [35]. The controlled hydration behavior, combined with the advantageous particle structure of 42.5 (described in Table 5 and visualized in Figure 5), directly confirms the denser and more homogeneous matrix structure observed in the SEM images (Figure 8). These combined effects provide a more uniform stress distribution throughout the composite, preventing premature failure.

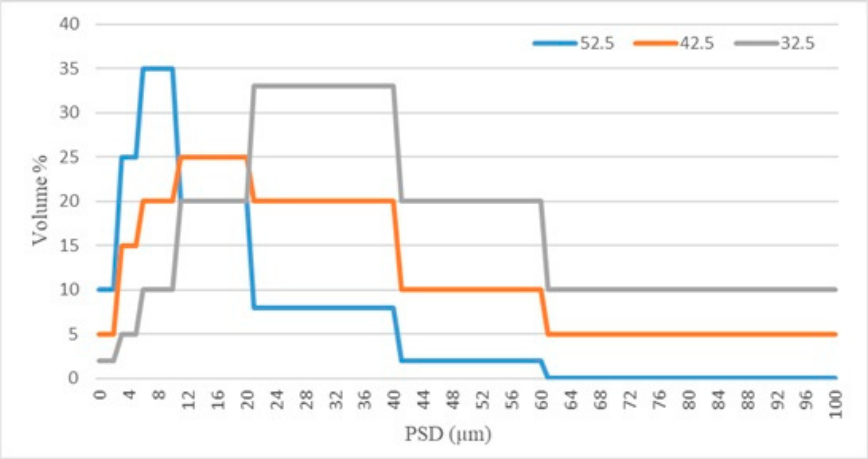


**Figure 5.** The analysis of the PSD of the cement types.

*3.6. Fourier Transform Infrared Spectroscopy*

FTIR analysis was conducted to characterize the chemical fingerprint of the composites and to understand the molecular interactions at the fiber-cement interface (Figure 6). The spectra reveal a distinct combination of organic and inorganic phases. The wood fibers are identified by O-H stretching (~3300 $cm^{-1}$) [36], C-H stretching (~2900 $cm^{-1}$) [37], hemicellulose C=O vibrations (~1730 $cm^{-1}$) [38], and lignin aromatic rings (~1600/1510 $cm^{-1}$) [37]. Simultaneously, the cementitious matrix is evidenced by the sharp $Ca(OH)_2$ peak (~3640 $cm^{-1}$) [34,39] and, most critically, the broad Si-O stretching band of the C-S-H gel (900-1000 $cm^{-1}$) [40,41], which is the primary source of mechanical strength.

To move beyond qualitative observation, the intensity ratios of key Si-O and Al-O peaks were calculated to quantify the degree of hydration (Table 6). This quantitative analysis provides the chemical validation for the mechanical superiority of the 42.5 cement discussed in previous sections.

**Table 6.** The Si-O and Al-O peak intensity ratios of composites based on cement type and fiber ratio.

| Cement Type | Fiber/Cement Ratio | Si-O (1200 $cm^{-1}$) | Si-O (1100 $cm^{-1}$) | Total Si-O | Al-O (820 $cm^{-1}$) | Al-O (680 $cm^{-1}$) | Total Al-O |
|---|---|---|---|---|---|---|---|
| 32.5 | 1/2 | 0.010 | 0.030 | 0.040 | 0.007 | 0.007 | 0.014 |
| | 1/3 | 0.053 | 0.053 | 0.106 | 0.032 | 0.049 | 0.081 |
| | 1/4 | 0.008 | 0.016 | 0.024 | 0.013 | 0.024 | 0.037 |
| | 1/5 | 0.013 | 0.020 | 0.033 | 0.017 | 0.021 | 0.038 |
| 42.5 | 1/2 | 0.008 | 0.009 | 0.017 | 0.001 | 0.001 | 0.002 |
| | 1/3 | 0.012 | 0.025 | 0.037 | 0.025 | 0.030 | 0.055 |
| | **1/4** | **0.130** | **0.330** | **0.460** | **0.034** | **0.067** | **0.101** |

 doi:10.20944/preprints202601.2020.v1



| | | | | | | | |
|---|---|---|---|---|---|---|---|
| | 1/5 | 0.025 | 0.036 | 0.061 | 0.021 | 0.033 | 0.054 |
| 52.5 | 1/2 | 0.012 | 0.012 | 0.024 | 0.000 | 0.003 | 0.003 |
| | 1/3 | 0.007 | 0.013 | 0.020 | 0.025 | 0.025 | 0.050 |
| | 1/4 | 0.007 | 0.019 | 0.026 | 0.023 | 0.035 | 0.058 |
| | 1/5 | 0.016 | 0.024 | 0.040 | 0.022 | 0.035 | 0.057 |

The most significant finding is the total Si-O intensity ratio of 0.46 achieved by the 42.5 cement at the 1/4 fiber/cement ratio. This value is substantially higher than that of any other group, indicating that this specific formulation facilitated the most extensive polymerization of C-S-H gel. This chemical evidence directly explains why this group achieved the peak MOR of 12.77 N/mm²; the 42.5 cement formed a denser, more developed hydration network that effectively encapsulated the fibers.

In contrast, increasing the fiber ratio to 1/2 resulted in drastically lower Si-O intensities across all cement types (e.g., dropping to 0.017 for 42.5). This confirms that excessive organic content inhibits the hydration reaction and prevents the formation of a continuous binding matrix, leading to the poor mechanical performance observed (MOR < 3 N/mm²).

A similar trend was observed in the aluminate phases (peaks at 820 and 680 $cm^{-1}$), which contribute to early strength and pore filling. The 42.5 cement (1/4 ratio) again exhibited the highest total Al-O intensity (0.101), suggesting a robust formation of C-A-H or C-A-S-H phases. Conversely, the 52.5 cement at the 1/2 ratio showed negligible aluminate formation (0.003), pointing to retarded hydration kinetics in the presence of high fiber content.

In summary, the FTIR data confirms that material performance is driven by an optimal chemical balance rather than just cement grade. The 42.5 cement at a 1/4 ratio represents a "chemical sweet spot," maximizing both silicate and aluminate hydration products to create a superior fiber-matrix bond.

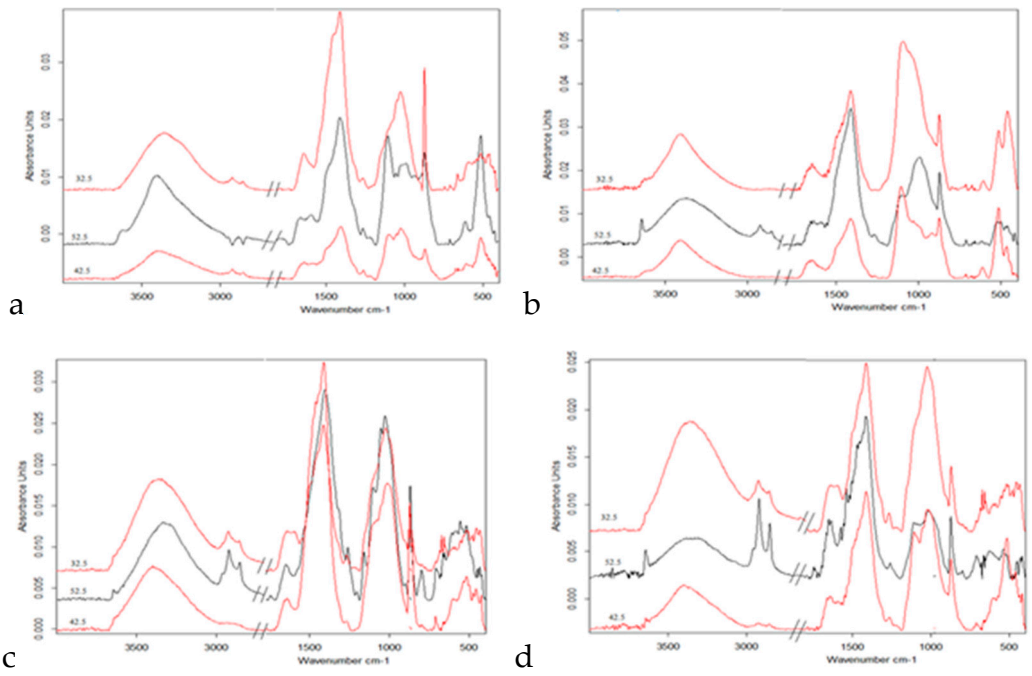


**Figure 6.** Effects of fiber / cement ratio and cement type on FT-IR of the boards. a: 1/2 fiber ratio CFB; b:1/3 fiber ratio CFB; c:1/4 fiber ratio CFB; d: 1/5 fiber ratio CFB.

*3.7. X-Ray Diffraction*

 doi:10.20944/preprints202601.2020.v1



The mineralogical composition of the produced boards was analyzed to visualize the crystalline and amorphous phases formed within the matrix (Figure 7). The diffraction patterns reveal a complex microstructure composed of hydration products and unreacted clinker phases.

The most critical feature for mechanical performance is the broad amorphous "hump" observed between 20° and 35° 2θ. This feature corresponds to the poorly crystalline Calcium Silicate Hydrate (C-S-H) gel, the primary binding agent in cementitious systems [29,42]. As seen in Figure 7, this amorphous hump is significantly more pronounced and intense in the 42.5 and 52.5 cement samples compared to the 32.5 type. This increased intensity serves as direct physical evidence that higher strength class cements generate a denser and more voluminous C-S-H gel network, which is essential for binding the wood fibers.

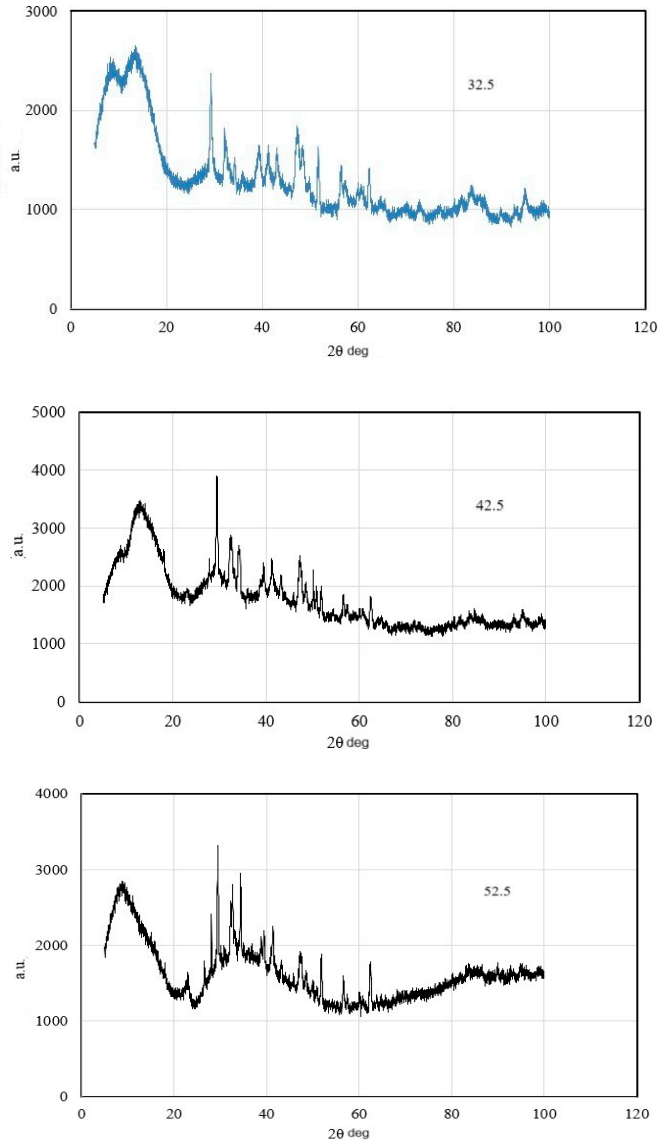


**Figure 7.** The XRD diffraction patterns of fiber cement boards (fiber-cement ratio 1/4).

Superimposed on this amorphous background are distinct crystalline peaks. The sharp reflection at 34.1° 2θ is identified as Portlandite ($Ca(OH)_2$), a key byproduct of hydration [27]. The stronger presence of this peak in the 42.5 and 52.5 samples further confirms a more advanced degree of hydration compared to the 32.5 cement. Additionally, peaks at 29.4° and 48.5° 2θ indicate the presence of Calcite ($CaCO_3$), suggesting that a portion of the hydration products underwent carbonation through reaction with atmospheric $CO_2$ during the curing process.

 doi:10.20944/preprints202601.2020.v1



***Correlation with Chemical and Mechanical Findings:*** These XRD results do more than just identify mineral phases; they provide the missing structural link connecting our chemical data to the final mechanical performance. We are essentially seeing a convergence of evidence across three different scales. The potential for strong gel formation, which we first identified through the high $CaO/SiO_2$ ratios and intense Si-O vibrations in the FTIR analysis, is physically confirmed by the prominent amorphous "hump" in the XRD patterns. This proves that the chemical potential was successfully translated into a physical reality: a dense C-S-H network. This microstructure is not merely a theoretical feature; it is the direct reason why the 42.5 and 52.5 groups achieved such superior mechanical strength (Table 4). For the optimal 42.5 sample (1/4 ratio) in particular, the XRD data completes the picture: it confirms that the high bond density detected chemically has materialized into a solid, load-bearing structure capable of delivering the high strength (12.77 $N/mm^2$) we observed [27].

### *3.8. Scanning Electron Microscope*

SEM imaging was utilized to visually evaluate the fiber-matrix interface, which is the critical stress-transfer zone determining the composite's ultimate strength. Figure 8 presents the surface morphology of the boards produced with different cement grades at the reference 1/4 ratio.

The microstructure of the 32.5 cement samples reveals the physical reasons behind their poor mechanical performance. As seen in Figure 8, the wood fibers are only partially encapsulated by the matrix. The texture is coarse and porous, with visible gaps at the fiber-cement interface. This lack of intimate bonding creates weak points where stress cannot be effectively transferred from the matrix to the fiber, simultaneously providing pathways for water ingress. This visual evidence directly correlates with the high water absorption and low MOR values reported earlier [3].

In contrast, the 52.5 cement samples exhibit a much denser morphology with improved fiber wrapping. However, the 42.5 cement samples display the most superior microstructure. Here, the distinction between fiber and matrix becomes blurred; the fibers are fully embedded within a compact, continuous hydration product network. This "seamless integration" suggests that the C-S-H gel has nucleated directly on the fiber surfaces, minimizing interfacial voids.

***Microstructural Validation of Multi-Scale Analysis:*** These micrographs effectively bridge the gap between our spectroscopic data and the physical performance of the boards. The dense, cohesive matrix we observe in the 42.5 samples is essentially the physical manifestation of the intense Si-O bonding and amorphous C-S-H phases previously identified in the FTIR and XRD analyses. This visual evidence clarifies the mechanism behind the mechanical results: the superior encapsulation of fibers seen in the SEM images ensures efficient load transfer from the matrix to the reinforcement. This strong interfacial bonding is the primary reason why the 42.5 group exhibited the highest stiffness and strength. Conversely, the visible porosity and poor fiber wetting in the 32.5 samples provide a clear structural explanation for their lower mechanical resistance and increased water absorption [29].

 doi:10.20944/preprints202601.2020.v1



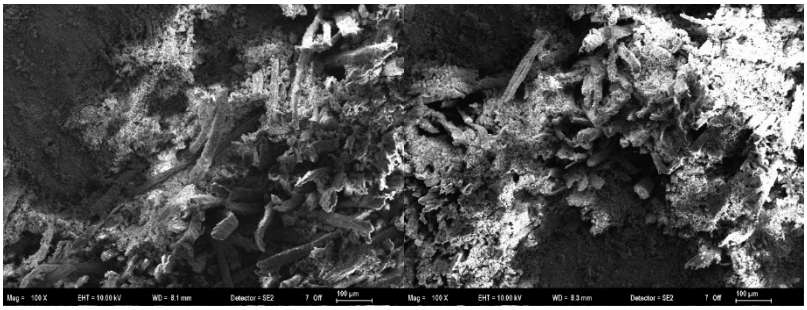

32.5 52.5

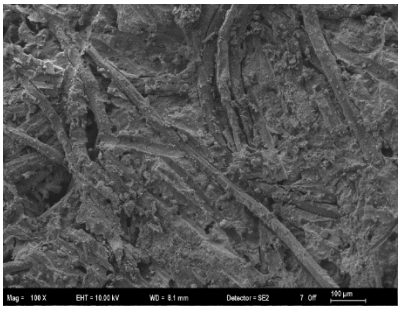

42.5

**Figure 8.** SEM images of fiber cement boards (fiber-cement ratio 1/4).

## 4. Conclusions

This study examined the effects of different cement types and fiber/cement ratios on the physical, mechanical, and thermal properties of cement-bonded fiberboards. The results clearly indicate that the fiber ratio is the governing factor that dictates the balance between mechanical strength and thermal insulation. We observed a distinct inverse relationship between these properties; while reducing the fiber ratio (from 1/2 to 1/5) significantly improved mechanical strength and dimensional stability, it naturally reduced the thermal insulation capacity. This is primarily because the higher cement content in low-ratio boards creates a denser matrix that effectively encapsulates the fibers, whereas the high-ratio boards benefit from the natural insulating properties of wood but suffer from increased porosity.

Among the tested parameters, the 42.5 cement type at a 1/4 fiber/cement ratio provided the most balanced performance, yielding high MOR and MOE values while maintaining acceptable physical properties. These macroscopic findings are strongly supported by the microstructural analyses conducted in this study. The FTIR and XRD data confirmed that the superior performance of the 42.5 samples stems from the formation of a dense C-S-H gel network. Furthermore, SEM imaging visually validated that at the optimal 1/4 ratio, the fibers were thoroughly encapsulated by the hydration products with minimal interfacial voids. This strong fiber-matrix bonding is the physical mechanism responsible for the effective load transfer and resistance to moisture ingress observed in the mechanical tests.

Consequently, the design of CFB should be driven by the specific target application rather than a single universal formula. For structural or exterior applications where high strength and moisture resistance are required, a lower fiber ratio (such as 1/4) combined with 42.5 cement is the ideal choice. Conversely, for non-load-bearing partition walls where thermal efficiency is the priority, higher fiber ratios can be utilized. These findings provide a practical scientific basis for the industry to develop purpose-driven and sustainable building materials.

**Author Contributions: Author Contributions:** Conceptualization, E.A, S.S.A. and E.G.; methodology, E.G., E.A and S.S.A.; validation, E.G.; formal analysis, E.G.; investigation, E.A and S.S.A.; resources, E.G.; data curation, E.A and S.S.A.; writing—original draft preparation, S.S.A.; writing—review and editing,E.A., S.S.A. and E.G.;

 doi:10.20944/preprints202601.2020.v1



visualization, S.S.A.; supervision, E.G. All authors have read and agreed to the published version of the manuscript.

**Funding:** This research received no external funding.

**Data Availability Statement:** The original contributions presented in the study are included in the article; further inquiries can be directed to the corresponding author.

**Acknowledgments:** The authors would like to thank the staff of the Department of Forest Industry Engineering at Bursa Technical University for their technical assistance during the experimental studies. During the preparation of this manuscript, the authors used AI-based tools (ChatGPT/Gemini) for English language editing and grammatical refinement. The authors have reviewed and edited the output and take full responsibility for the content of this publication.

**Conflicts of Interest:** The authors declare no conflict of interest. The funders had no role in the design of the study; in the collection, analyses, or interpretation of data; in the writing of the manuscript; or in the decision to publish the results.

## Abbreviations

The following abbreviations are used in this manuscript:

PC: Portland cement
$CaCl_2$: Calcium chloride
CFB: Cement fiber board
C-S-H: Calcium silicate hydrate
d: Density
FTIR: Fourier transform ınfrared spectroscopy
ITZ: Interfacial transition zone
MC: Moisture content
MOE: Modulus of elasticity
MOR: Modulus of rupture
PSD: Particle size distribution
SEM: Scanning electron microscopy
TC: Thermal conductivity
TS: Thickness swelling
WA: Water absorption
XRD: X-ray Diffraction
XRF: X-ray fluorescence

## References

1. Soroushian, P.; Aouadi, F. Mechanical properties of cement composites reinforced with polypropylene fibers. ACI Mater. J. 1992, 89, 170–176.
2. Coutts, R.S.P. A review of Australian research into natural fibre cement composites. Cem. Concr. Compos. 2005, 27, 518–526.
3. Hasan, K.F.; Horváth, P.G.; Bak, M.; Alpár, T. A state-of-the-art review on coir fiber-reinforced biocomposites. RSC Adv. 2021, 11, 10548–10571.
4. Wang, L.; Chen, S.S.; Tsang, D.C.; Poon, C.S.; Shih, K. Value-added recycling of construction waste wood into noise and thermal insulating cement-bonded particleboards. Constr. Build. Mater. 2016, 125, 316–325.
5. Lorimer, M. Estimating the Acoustic Absorption of Wood-Infused Concretes. Ph.D. Thesis, University of Ottawa, Ottawa, ON, Canada, 2023.
6. Liu, F.; Chen, G.; Li, L.; Guo, Y. Study of impact performance of rubber reinforced concrete. Constr. Build. Mater. 2012, 36, 604–616.

 doi:10.20944/preprints202601.2020.v1




7. Allen, A.J.; Thomas, J.J.; Jennings, H.M. Composition and density of nanoscale calcium–silicate–hydrate in cement. Nat. Mater. 2007, 6, 311–316.
8. Nasr, D.; Behforouz, B.; Borujeni, P.R.; Borujeni, S.A.; Zehtab, B. Effect of nano-silica on mechanical properties and durability of self-compacting mortar containing natural zeolite: Experimental investigations and artificial neural network modeling. Constr. Build. Mater. 2019, 229, 116888.
9. Okino, E.Y.A.; de Souza, M.R.; Santana, M.A.E.; Alves, M.V.S.; de Sousa, M.E.; Teixeira, D.E. Cement-bonded wood particle-board with a mixture of eucalypt and bamboo. Cem. Concr. Compos. 2004, 26, 729–734.
10. Amiandamhen, S.O.; Meincken, M.; Tyhoda, L. The effect of chemical treatments of natural fibres on the properties of phosphate-bonded composite products. Wood Sci. Technol. 2018, 52, 653–675.
11. Frybort, S.; Mauritz, R.; Teischinger, A.; Müller, U. Cement bonded composites—A mechanical review. BioResources 2008, 3, 602–626.
12. Liu, J.; Lv, C. Research progress on durability of cellulose fiber-reinforced cement-based composites. Int. J. Polym. Sci. 2021, 2021, 1014531.
13. Fuwape, J.A.; Fabiyi, J.S.; Osuntuyi, E.O. Technical assessment of three-layered cement-bonded boards produced from wastepaper and sawdust. Waste Manag. 2007, 27, 1611–1616.
14. Taylor, H.F. Cement Chemistry, 2nd ed.; Thomas Telford: London, UK, 1997; Volume 2, p. 459.
15. Mindess, S. Resistance of concrete to destructive agencies. In Lea's Chemistry of Cement and Concrete; Hewlett, P.C., Liska, M., Eds.; Butterworth-Heinemann: Oxford, UK, 2019; pp. 251–283.
16. Scrivener, K.; Ouzia, A.; Juilland, P.; Mohamed, A.K. Advances in understanding cement hydration mechanisms. Cem. Concr. Res. 2019, 124, 105823.
17. Bentur, A.; Mindess, S. Fibre Reinforced Cementitious Composites, 2nd ed.; CRC Press: Boca Raton, FL, USA, 2006.
18. De Brito, J.; Agrela, F., Eds. New Trends in Eco-Efficient and Recycled Concrete; Woodhead Publishing: Cambridge, UK, 2018.
19. Castillo-Lara, J.F.; Flores-Johnson, E.A.; Valadez-Gonzalez, A.; Herrera-Franco, P.J.; Carrillo, J.G.; Gonzalez-Chi, P.I.; Li, Q.M. Mechanical properties of natural fiber reinforced foamed concrete. Materials 2020, 13, 3060.
20. Robert, U.W.; Etuk, S.E.; Agbasi, O.E.; Ambrose, P.D. Development of lightweight sawdust-based composite panels for building purposes. Int. J. Lightweight Mater. Manuf. 2024, 7, 631–640.
21. Wei, Y.M.; Tomita, B. Effects of five additive materials on mechanical and dimensional properties of wood cement-bonded boards. J. Wood Sci. 2001, 47, 437–444.
22. Abdollahiparsa, H.; Shahmirzaloo, A.; Teuffel, P.; Blok, R. A review of recent developments in structural applications of natural fiber-reinforced composites (NFRCs). Compos. Adv. Mater. 2023, 32, 26349833221147540.
23. Biskri, Y.; Babouri, L.; Boukhelf, F.; Charradi, K.; Annaba, K.; El Mendili, Y. On the physical-mechanical behavior of fiber cement composite: Effect of chemical treatment of sisal fibers. J. Build. Eng. 2025, 101, 111978.
24. Mehta, P.K.; Monteiro, P.J. Concrete Microstructure, Properties, and Materials, 3rd ed.; McGraw-Hill: New York, NY, USA, 2006.
25. Rowell, R.M. Handbook of Wood Chemistry and Wood Composites; CRC Press: Boca Raton, FL, USA, 2005.
26. Sofi, A. Effect of waste tyre rubber on mechanical and durability properties of concrete–A review. Ain Shams Eng. J. 2018, 9, 2691–2700.
27. Soroushian, P.; Balachandra, A.; Nassar, S.; Weerasiri, R.; Darsanasiri, N.; Abdol, N. Effect of fiber type and content on the performance of extruded wood fiber cement products. Case Stud. Constr. Mater. 2022, 16, e00968.
28. Aloulou, F.; Sammouda, H. Thermal conductivity and mechanical properties of organo-clay-wood fiber in cement-based mortar. In Sand in Construction; IntechOpen: London, UK, 2022.
29. Ferreira, S.R.; de Andrade Silva, F.; Lima, P.R.L.; Toledo Filho, R.D. Effect of fiber treatments on the sisal fiber properties and fiber–matrix bond in cement based systems. Constr. Build. Mater. 2015, 101, 730–740.

 doi:10.20944/preprints202601.2020.v1



30. Neville, A.M. Properties of Concrete, 5th ed.; Pearson: London, UK, 2011.
31. De Larrard, F. Concrete Mixture Proportioning: A Scientific Approach; CRC Press: London, UK, 1999.
32. Wong, H.H.C.; Kwan, A.K.H. Packing density of cementitious materials: Part 1—Measurement and modelling. Mater. Struct. 2008, 41, 655–671.
33. Bishnoi, S.; Scrivener, K.L. A model for the microstructure of cement hydration. Cem. Concr. Res. 2009, 39, 73–83.
34. Lothenbach, B.; Winnefeld, F.; Alder, C.; Wieland, E.; Lunk, P. Effect of temperature on the pore solution, microstructure and hydration products of Portland cement pastes. Cem. Concr. Res. 2007, 37, 483–491.
35. Siddique, R.; Khan, M.I. Supplementary Cementing Materials; Springer: Berlin/Heidelberg, Germany, 2011.
36. Pandey, K.K.; Pitman, A.J. FTIR studies of the changes in wood chemistry during weathering. Wood Sci. Technol. 2003, 37, 239–249.
37. Faix, O. Classification of lignins from different botanical origins by FT-IR spectroscopy. Holzforschung 1991, 45, 21–27.
38. Colom, X.; Carrillo, F.; Nogués, F.; Garriga, P. Structural analysis of photodegraded wood by means of FTIR spectroscopy. Polym. Degrad. Stab. 2003, 80, 543–549.
39. Wu, J.; Wan, C.; Hong, Z.; Zhou, A.; Tan, Y.; Deng, Y. Insights into clinker-clay interactions in stabilized soft clay using NMR, TEM, and FTIR. J. Rock Mech. Geotech. Eng. 2024, in press. doi:10.1016/j.jrmge.2024.11.037.
40. Richardson, I.G. The nature of CSH in hardened cements. Cem. Concr. Res. 1999, 29, 1131–1147.
41. Qin, L.; Gao, X.; Chen, T. Influence of mineral admixtures on carbonation curing of cement paste. Constr. Build. Mater. 2019, 212, 653–662.
42. Tang, B.; Fan, M.; Yang, Z.; Sun, Y.; Yuan, L. A comparison study of aggregate carbonation and concrete carbonation for the enhancement of recycled aggregate pervious concrete. Constr. Build. Mater. 2023, 371, 130797.